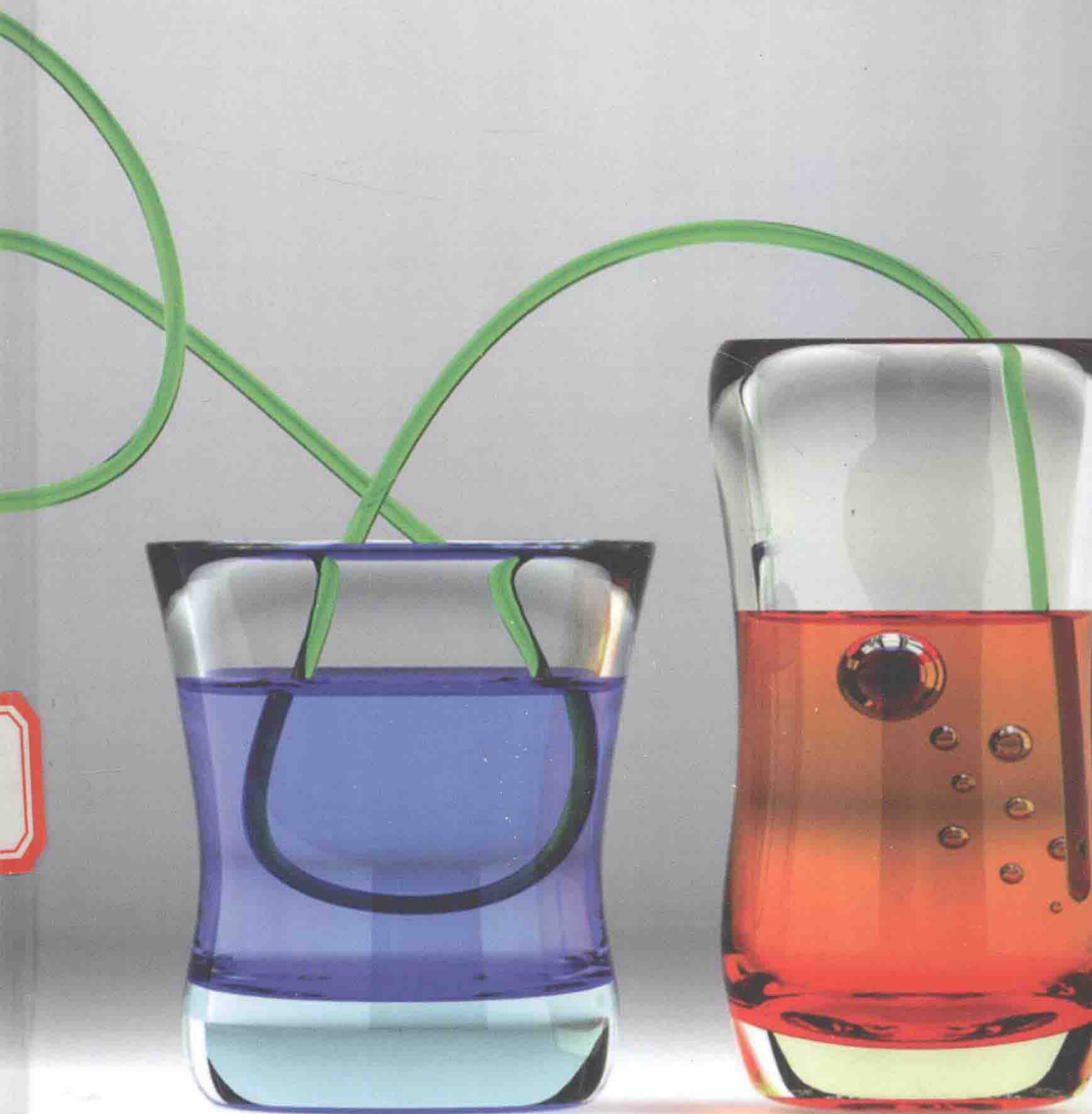


Principles and Practice of **Fluid Mechanics**

Fay McGuire



Principles and Practice of Fluid Mechanics

Edited by **Fay McGuire**

NYRESEARCH
P R E S S

New York

Published by NY Research Press,
23 West, 55th Street, Suite 816,
New York, NY 10019, USA
www.nyresearchpress.com

Principles and Practice of Fluid Mechanics

Edited by Fay McGuire

© 2015 NY Research Press

International Standard Book Number: 978-1-63238-372-3 (Hardback)

This book contains information obtained from authentic and highly regarded sources. Copyright for all individual chapters remain with the respective authors as indicated. A wide variety of references are listed. Permission and sources are indicated; for detailed attributions, please refer to the permissions page. Reasonable efforts have been made to publish reliable data and information, but the authors, editors and publisher cannot assume any responsibility for the validity of all materials or the consequences of their use.

The publisher's policy is to use permanent paper from mills that operate a sustainable forestry policy. Furthermore, the publisher ensures that the text paper and cover boards used have met acceptable environmental accreditation standards.

Trademark Notice: Registered trademark of products or corporate names are used only for explanation and identification without intent to infringe.

Printed in China.

Preface

The world is advancing at a fast pace like never before. Therefore, the need is to keep up with the latest developments. This book was an idea that came to fruition when the specialists in the area realized the need to coordinate together and document essential themes in the subject. That's when I was requested to be the editor. Editing this book has been an honour as it brings together diverse authors researching on different streams of the field. The book collates essential materials contributed by veterans in the area which can be utilized by students and researchers alike.

Fluid mechanics is a complicated and extremely challenging field of study. It is central to several matters that are significant not only technologically, but also sociologically. This book emphasizes on a cross-section of procedures in fluid mechanics, each of which explains new ideas and relates to one or more matters of high interest during the early 21st century. The challenges constitute multi-phase flows, compressibility, non-linear dynamics, flow instability, transforming solid-fluid boundaries and fluids with solid-like characteristics. The procedures relate difficulties like weather and climate forecast, health care, efficiency of fuel, wind/wave energy harvesting, air quality, erosion, lessening landslides and noise.

Each chapter is a sole-standing publication that reflects each author's interpretation. Thus, the book displays a multi-facetted picture of our current understanding of application, resources and aspects of the field. I would like to thank the contributors of this book and my family for their endless support.

Editor

Contents

	Preface	VII
	Part 1 General Fluid Mechanical Methods	1
Chapter 1	Overview on Stereoscopic Particle Image Velocimetry L. Martínez-Suástegui	3
	Part 2 Illustrative Applications	21
Chapter 2	Two-Dimensional Supersonic Flow with Perpendicular Injection of the Gas Ye. Belyayev and A. Naimanov	23
	Part 3 Advances in Classical Approaches	45
Chapter 3	Parallel Accelerated Group Iterative Algorithms in the Solution of Two-Space Dimensional Diffusion Equations Norhashidah Hj Mohd Ali and Foo Kai Pin	47
Chapter 4	An Idealised Biphasic Poroelastic Finite Element Model of a Tibial Fracture Sanjay Mishra	71
Chapter 5	Dynamically Incompressible Flow Christopher Depcik and Sudarshan Loya	85
Chapter 6	Modification of the Charnock Wind Stress Formula to Include the Effects of Free Convection and Swell C.H. Huang	113
Chapter 7	Radial Basis Functions Methods for Solving Radionuclide Migration, Phase Change and Wood Charring Problems Leopold Vrankar, Franc Runovc and Goran Turk	137

Chapter 8	Simulation of Acoustic Sound Produced by Interaction Between Vortices and Arbitrarily Shaped Body in Multi-Dimensional Flows by the Vortex Method Yoshifumi Ogami	157
Part 4	Non-Classical Approaches	183
Chapter 9	Topology Optimization of Fluid Mechanics Problems Maatoug Hassine	185
Chapter 10	Multiscale Particle-In-Cell Method: From Fluid to Solid Mechanics Alireza Asgari and Louis Moresi	207
	Permissions	
	List of Contributors	

Part 1

General Fluid Mechanical Methods

Overview on Stereoscopic Particle Image Velocimetry

L. Martínez-Suástegui

*ESIME Azcapotzalco, Instituto Politécnico Nacional, Colonia Santa Catarina,
Delegación Azcapotzalco, México, Distrito Federal,
Mexico*

1. Introduction

Recently, Particle Image Velocimetry (PIV) has become the method of choice for multiple fluid-dynamic investigations (Adrian 1991; Willert and Gharib 1991; Jakobsen, Dewhurst et al. 1997; Westerweel 1997; Raffel, Willert et al. 1998). PIV is a reliable non-intrusive laser optical measurement technique that is based on seeding a flow field with micron-sized tracer particles and illuminating a two-dimensional (2D) slice or target area with a laser light sheet (Adrian and Yao 1985; Melling 1997). The target area is captured onto the sensor array of a digital camera, which is able to capture each light pulse in separate image frames. After recording a sequence of two light pulses, velocity vectors are derived from small subsections (called interrogation areas) of the target area of the particle-seeded flow by measuring the distance travelled by particles in the flow within a known time interval. The interrogation areas from the two image frames are cross-correlated with each other, pixel by pixel, producing a signal peak that allows for an accurate measurement of the displacement, and thus the velocity. Finally, the instantaneous velocity vector map over the whole target area is obtained by repeating the cross-correlation for each interrogation area over the two image frames captured by the camera (Nishino, Kasagi et al. 1989; Keane and Adrian 1992; Mao, Halliwell et al. 1993; Westerweel, Dabiri et al. 1997). The major drawback of the 2D PIV technique is that it records only the projection of the velocity vector into the plane illuminated by the laser sheet, so the out-of-plane velocity component is lost and the in-plane components are affected by an unrecoverable error due to the perspective transformation. Although the “classical” PIV method introduces an error due to the perspective projection and uncertainty in measuring the in-plane velocity components, most of the time it is commonly neglected, since it still allows the user to interpret the instantaneous flow field and its structures (Lawson and Wu 1997; Lawson and Wu 1997; Soloff, Adrian et al. 1997). Unfortunately, this is not the case when studying highly three-dimensional flows, where the only way to avoid the uncertainty error is to measure all three components of the velocity vectors using stereoscopic techniques (Adrian 1991; Arroyo and Greated 1991; Westerweel and Nieuwstadt 1991; Hinsch 1993; Prasad and Adrian 1993; Raffel, Gharib et al. 1995; Lawson and Wu 1999; Prasad 2000; Doorne 2004; Tatum, Finnis et al. 2005; Mullin and Dahm 2006; Tatum, Finnis et al. 2007). Stereoscopic PIV uses two cameras with separate viewing angles. By combining the two velocity fields measured by

each camera using geometrical equations derived from the camera setup and a complicated calibration step, the third velocity component is evaluated and a three-dimensional (3D) velocity field is achieved (Nishino, Kasagi et al. 1989; Grant, Zhao et al. 1991; Raffel, Gharib et al. 1995; Willert 1997; Kähler and Kompenhans 2000; Shroder and Kompenhans 2004; Mullin and Dahm 2005; Perret, Braud et al. 2006).

In the present chapter, the technical basis, the set-up and components of a stereoscopic PIV apparatus/equipment are described so that the reader can understand how the different items of equipment are combined to form a coherent PIV tool (Hu, Saga et al. 2001). Afterwards, the principles of stereo PIV calibration, data acquisition, processing, and analysis are addressed. The aim of this chapter is to present in a more general context the aspects of the PIV technique relevant for those who intend to purchase a stereoscopic PIV system or those who want to perform stereoscopic PIV measurements. By understanding how to plan and perform experiments, it is hoped that it will allow the reader to successfully design a custom measurement system to fit a specific scientific or industrial application. In addition, this chapter will prove a valuable tool for those who already own a 2D PIV system and want to upgrade it for 3D measurement acquisition.

2. PIV system overview

There are several commercial stereoscopic PIV systems available, but the basic elements of these systems must include the following items: a pulsed laser system, two cameras for stereoscopic measurements, and a PC connected to a data acquisition card that synchronizes all of these items. The instrumentation required to perform the PIV data acquisition process is seeding, illuminating, recording, processing, and analysing the flow field. One drawback of PIV systems is that all of these items contribute to each stage of the measurement process, and therefore none of them can be spared. A brief description of the aforementioned instrumentation is presented in the following subsections.

2.1 Illumination systems

A stroboscopic light-sheet is desired to illuminate the plane of interest. This can be generated with pulsed lasers, continuous wave lasers, electro-optical shutters, polygon scanners, light guides and optical assemblies. Since only pulsed lasers have sufficient energy to record particle images, for relatively high speed flows seeded with micron or submicron particles, the most common choice are Nd:Yag lasers with a wavelength of 532 nm, since they offer repetition rates that match most of the commercially available CCD cameras. Pulsed laser systems include an array of optics with several cylindrical lenses that produces a diverging light sheet with adjustable thickness. This optical system includes an optical mount that can rotate through 360°. One thing to remember when designing experiments is that in order to avoid damage to the equipment, the laser must always be mounted and operated in a horizontal position. The sheet can be easily oriented by deflecting the laser beam using a mirror. Also, when it comes to choosing a pulsed laser for a stereo PIV system, the most important specifications to account for are: minimum sheet thickness range, the sheet focusing range, the maximum input pulse energy, the maximum input beam diameter, and of course its dimensions. The laser of choice must suit the measurement of the particular flow field under investigation. Nevertheless, when purchasing a PIV system, always aim for a laser with the maximum laser power output.

2.2 Cameras

Several CCD-based cameras are currently available. They differ in the desired spatial resolution, temporal resolution, directional ambiguity resolution, and cross-correlation options. Again, the cameras of choice depend on the resolution of the spatial and temporal features of the flow field to be measured. Generally, as the spatial resolution of the camera increases, its temporal resolution decreases. Therefore, when customizing your PIV equipment, always make sure that the chosen cameras meet the following criteria. They have enough temporal resolution in order to resolve the smallest velocity displacements between the first and second images of the particles of the flow field under investigation. The size of the smallest velocity structures can be measured in the flow field under study. One important thing to consider is that commercial PIV systems include a feature that interfaces the input buffer in the PIV processor with the cameras, thus allowing future upgrades of particular camera systems that better suit your needs. With that in mind, the best option when purchasing your first set of cameras for the PIV system is to make sure that they satisfy your particular needs in terms of temporal resolution with the highest spatial resolution.

2.3 Software to perform the PIV data acquisition process

The software of the PIV system must include a synchronization unit that links signals to and from the processor, the laser and cameras. Once the images have been acquired, the system must be able to produce and store vector maps or image maps in a database on a hard disc of a PC that keeps track of both the data and corresponding data acquisition and analysis parameters used.

2.4 3D traverse system

If the light sheet optics and the cameras are mounted on a common traverse system, they can be positioned at any desired point in the flow domain. This capability is particularly advantageous for measuring image data at multiple planes in a flow. Volume mapping is a technique based on performing multiple 3D stereoscopic PIV mappings in cross-sections of a flow within a very short time interval (Meinhart, Wereley et al. 2000; Klank, Goranovic et al. 2001). Unfortunately, this technique can only be used with a traverse system, and it is achieved by mounting the laser cavity and the cameras on an electronically controlled traverse system. In this way, when the entire traverse system is moved, the distance between the cameras and the light sheet remains constant so that there is no need to calibrate again. Although 2D or 3D PIV measurements can be performed without a traverse system, the main advantage of these systems is that they allow for fast and accurate calibration. For stereoscopic measurements in an enclosed flow (e.g., a duct flow, where the laser and cameras are outside of a transparent model), the index of refraction can have a strong effect on the calibration. One method to ensure that the two cameras have an orthogonal orientation with respect to the liquid-air interface is to redesign the wall of the test section to incorporate a triangular prismatic section. This is easily achieved by constructing a glass container that is filled with the same liquid and that is attached to the test section. By using a liquid prism between the test section and the lens of each camera, orthogonal viewing is accomplished with respect to the liquid-air interface and the aberrations are minimized (Prasad and Adrian 1993; Prasad and Jensen 1995). Also, when the test section has curved walls, distortion caused by refraction is minimized by enclosing the test section in a container with flat windows and filled with the same fluid as the test section.

3. Stereoscopic PIV calibration tools

In this section, the calibration tools for stereoscopic calibration and the calibration procedure are presented and described in detail.

3.1 Camera mounts for stereoscopic viewing

In most 3D PIV systems, when viewing the light sheet at an angle, the camera's entire field of view must be accurately focused. This is known as the Scheimpflug condition, and it is accomplished using camera mounts that include angle adjustment so that the image plane (CCD-plane), lens plane and object plane for each of the cameras intersect at a common point, as shown in Figure 1a (Scheimpflug 1904; Prasad and Jensen 1995; Zang and Prasad 1997). Figure 1b shows a camera mounted on a stereoscopic camera mount with angle adjustment and Scheimpflug condition.

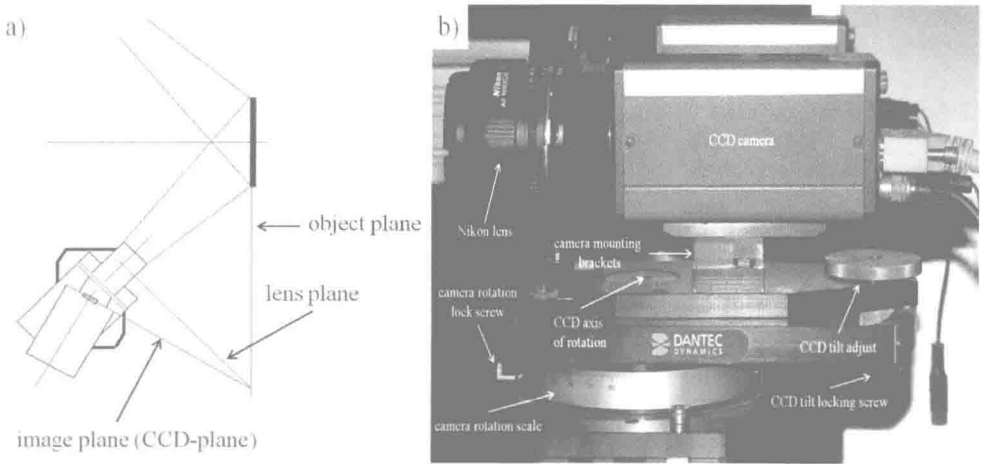


Fig. 1. a) Scheimpflug camera. b) CCD camera mounted on a Scheimpflug camera mount.

3.2 Calibration target

Stereo PIV measures displacements by using two cameras playing the role of eyes. By comparing the images of each camera against a calibration target, a stereoscopic calibration, which will be described in the next subsection, is achieved. Plane calibration targets consist of a one-sided white image with black dots on a regular spaced grid that is easily detected using image processing techniques (Harrison, Lawson et al. 2001; Ehrenfried 2002; Wieneke 2005). When these targets are used, the two cameras have to be positioned on the same side. On the other hand, double-sided (multi-level) targets contain a two-level grid of white dots on a black background located at two different and known orientations of the z -axis, where z is the distance away from the camera(s). One major advantage of these targets is that depending on the configuration of the experimental setup, the user can choose to mount the cameras either on opposite sides of the calibration target or on the same side. Although small angles between the two cameras can be used, the out-of-plane displacement is obtained more accurately when a larger angle is used between the two cameras. In this sense, the most accurate calibration is obtained when the angle between the two cameras is

set to 90° (Sinha 1988; Westerweel and Nieuwstadt 1997). Nonetheless, stereoscopic PIV is also possible using a nonsymmetric arrangement of the cameras as long as the viewing axes are not collinear. Both types of targets have a larger centre dot called the “zero marker” which corresponds to the level at which the big dot in the centre of the calibration target is placed. Figure 2 shows the recommended setup for the cameras depending on the type of target used. Note that when the cameras have a narrow depth of field, a smaller separation angle will be needed to allow a wider field of view (i.e., where both cameras are in focus).

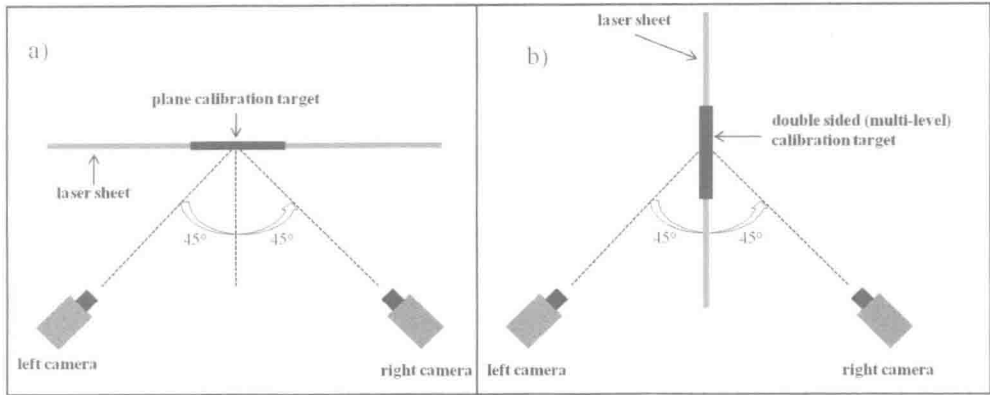


Fig. 2. Optimal camera configurations for an optimal determination of the stereoscopic calibration coefficients: a) Configuration using a plane (one-sided) calibration target. b) Configuration using a multi-level (two-sided) calibration target.

3.3 Calibration procedure

An imaging model describes the mapping of points from the image plane to object space, and the model parameters are determined through analysis of one or more calibration images. To obtain an imaging model, the first step is to accurately align the calibration target with the laser light sheet (Willert 1997). For 3D PIV measurements, the laser light thickness is adjusted by an optical arrangement supplied with the laser so that the illuminated plane is as thick as possible. If calibration is to be performed using a plane target, the cameras have to acquire images of the target through a number of z positions. This is generally accomplished by mounting the target on a special traverse unit and recording three to five z positions. Figure 3 shows the calibration grid images obtained by each camera for one z position using a plane calibration target of 100 x 100 mm with black dots and white background. The camera configuration corresponds to the one shown in Figure 2a). Multi-level double sided targets eliminate the need for traversing, since they contain a two-level grid of white dots on a black background with known dot spacing in the x,y and z positions. Figure 4 shows a multi-level target of 270 x 190 mm with white dots and black background. The alignment of the laser light sheet and the target depend on the camera configuration. If the cameras are located on opposite sides of a multi-level calibration target, then the laser light sheet has to be aligned with the centre of the target. Here, the $z=0$ coordinate is located at the centre of the laser light sheet. If the cameras are placed on the same side of the calibration target, the laser light sheet has to be positioned in the plane located in the middle of each level. In this case, the plane located at the centre of the light

sheet corresponds to the plane at which $z=0$. After aligning the calibration target, the user has to select the type of target used from a list. This setting allows the system to associate known x and y positions with the size and location of the markers, as the calibration algorithm automatically identifies the x and y coordinates on the images. The calibration target used during 3D stereo PIV measurements must always match the experimental setup, i.e. when measuring a large or small area, a large or small target is needed, respectively.

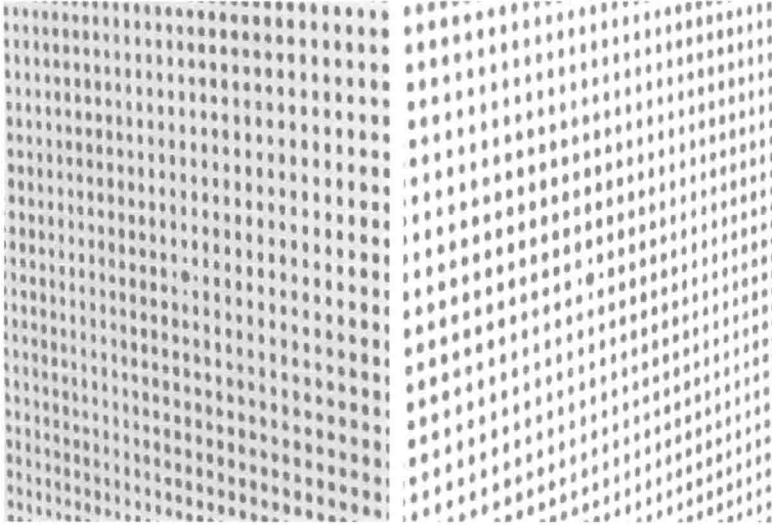


Fig. 3. Right and left calibration grid images obtained by each camera using a plane (one-sided) calibration target. The big dot in the centre of the calibration target is the zero marker.

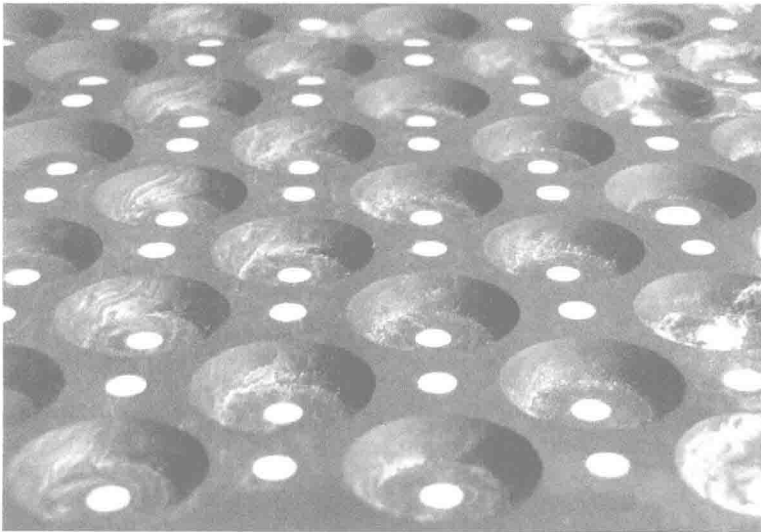


Fig. 4. Multi-level target of 270 x 190 mm with white dots and black background.

Once the type of target used for the calibration is entered, information such as dot spacing in the x , y coordinates, zero marker diameter, axis marker diameter and level distance are known. The next step is to define the coordinate axes as seen from the cameras' point of view and the target configuration. Here, the x , y and z axes are always horizontal, vertical, and normal to the light sheet, respectively. However, each can be positive in any direction so that eight different coordinate system combinations are available. To obtain the z calibration coefficient, each camera records images of the calibration target for several z positions by traversing it in a direction normal to the laser sheet. Each displacement value is entered by the user in the dataset properties, and this calibration stage determines the x - y image to object plane space mapping (Lawson and Wu 1997; Soloff, Adrian et al. 1997). Table 1 shows some of the available sizes for each type of target. Note that for the case of multi-level targets, the z -coordinate refers to the location of the zero marker and the z values entered correspond to the dots located on the second level. These values are added or subtracted depending on the level spacing of each target and on how the calibration target is aligned with the laser light sheet.

Type of calibration target	Size (mm)	Z values entered (mm)
Dots	100 x 100	-
Dots	200 x 200	-
Dots	270 x 200	-
Dots	450 x 450	-
Multi-level	270 x 190	2 nd level +4
Multi-level	270 x 190	2 nd level -4
Multi-level	95 x 75	2 nd level +2
Multi-level	95 x 75	2 nd level -2

Table 1. Available sizes for plane and multi-level calibration targets.

After the entry properties of the calibration images are set and saved, the obtained transformation describes the overall perspective and lens distortion by providing parameter values for a specific image acquisition setup called the “imaging model fit”. The calibration result can be verified by superimposing the model fit map to the corresponding calibration image. Figure 5 shows the imaging model for each camera based on an image size of 1344 x 1024 pixels after applying a direct linear transform and using a multi-level calibration target of 270 x 190 mm. The origin of the x , y and z coordinates is located at the centre of the zero marker and the coordinate axes are displayed as seen from each camera. The yellow dots at the centre of the white markers appear when a successful image model fit is obtained. Note that for both images, the Scheimpflug condition was not accomplished on the markers located at each corner. Nonetheless, a successful 3D calibration can still be obtained using an image model fit using sixteen out of the twenty available markers.

The quality of the calculated imaging model fit can be evaluated with the value of the average reprojection error. The latter describes the average pixel distance from every marker found to the predicted image location (distance from the yellow dots at the centre of the white markers to the points of intersection of the green grid in Figure 5). In this sense, the

accuracy of the image model fit increases as the value of the average reprojection error decreases, and normally accepted values lie below 0.5. After performing a successful 3D calibration, the calibration target is removed and stereo measurements can be acquired by processing 2D PIV simultaneous recordings from each camera using the scale factor based on the image model fit. The two 2D vector maps recorded by each camera are then post processed using standard PIV processing software to obtain 3D vector maps. The main advantage of 3D calibration is that since a direct mapping function is derived between an object in 3D space and its corresponding location in the in-planes, there is no need to provide information regarding the geometric parameters of the stereoscopic image acquisition (Prasad 2000).

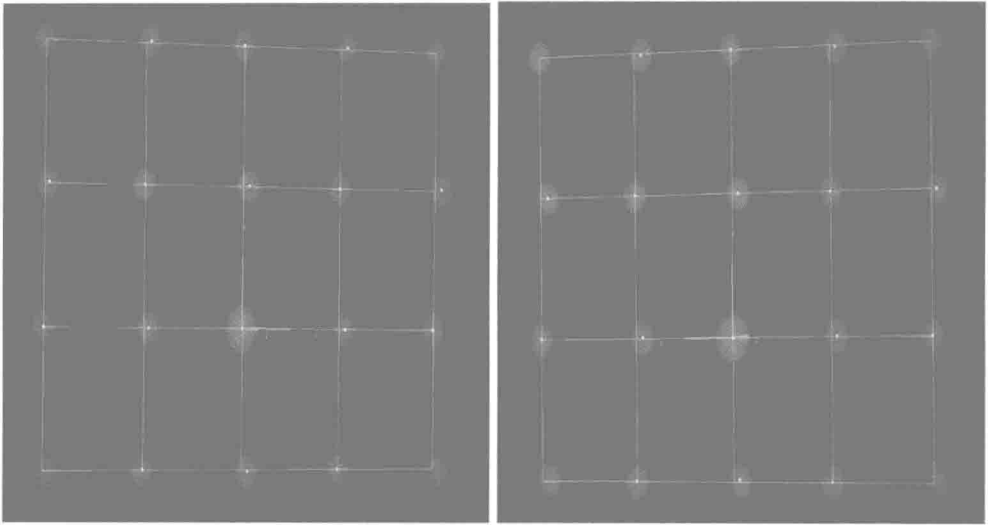


Fig. 5. Imaging model for each camera. The average reprojection errors are of 1.5544×10^{-1} and 2.2423×10^{-1} pixels for the left and right camera, respectively.

4. Data processing and analysis

This section describes how to perform 3D data processing and analysis after data acquisition, and addresses various options to export the processed information of the 3D image maps for further investigation and processing to spreadsheet displays, ASCII files, MATLAB or Tecplot 360.

4.1 Adaptive correlation

The adaptive correlation analysis method calculates velocity vectors starting with an initial interrogation area of size $m \times n$ pixels. After the first iteration, vectors are recalculated using a smaller interrogation area, and this procedure is repeated until a final interrogation area is reached. The number of iterations is specified by the user and it's called "number of refinement steps." The size of the final interrogation area is also specified by the user, and its value is determined by entering values of the horizontal and

vertical sides (in pixels) of the latter. For each direction, available sizes are of 8, 16, 32, 64, 128 and 254 pixels. The initial interrogation area size is obtained by multiplying the final interrogation area size times the number of refinement steps, e.g., when selecting 3 refinement steps using a final interrogation area of 16×16 pixels, the initial interrogation area size is of 128×128 pixels. To reduce the correlation anomalies, overlap between neighbour interrogation areas can be specified independently for the horizontal and vertical directions. Validation parameters for the adaptive correlation method are normally used to remove spurious vectors. One of these parameters is the “peak validation.” Here, the user sets values for the minimum and maximum peak widths as well as the minimum peak height ratio between the first and second peak. The “local neighbourhood validation” rejects spurious vectors and replaces them using a linear interpolation method based on the surrounding vectors located at an area of $m \times n$ pixels set by the user. Note that spurious vectors are identified by the inputted value of the “acceptance factor” parameter, and for larger values of this parameter, less velocity vectors are spatially corrected. The “moving average validation” method is used to validate vector maps by comparing each vector with the average of other vectors in a defined neighbourhood. Vectors that deviate from specified criteria are replaced using the average of the surrounding vectors. Figure 6 illustrates how the calculated velocity vectors obtained after applying an adaptive correlation can vary depending on the values of the input parameters described above. The computed vectors are displayed in blue, while the green vectors correspond to those obtained after interpolation with the surrounding vectors. This figure exemplifies the importance of adequately setting the values of the interrogation areas and validation methods employed. The instantaneous velocity map shown in Figure 6 is the recorded instantaneous flow structure of a free falling rotary seed that’s spinning at a stationary height inside a low-speed, vertical wind tunnel crafted for studying its flow and kinematics. Velocity measurements were performed using a Dantec Dynamics DSPIV system and the images were processed using Dantec Dynamics software (DynamicStudio version 3.0.69). Seeding was supplied from a smoke generator (Antari Z-1500II Fog Machine, Taiwan, ROC) placed at the tunnel intake, and seeding quantity was regulated by monitoring the output from the DSPIV system (particle size $1 \mu\text{m}$). To elucidate the effects of the value of the input parameters, the recipe for the left and right adaptive correlations of Figure 6 are displayed on the left and right sides of Figure 7, respectively.

The adaptive correlation on the left of Figure 6 used the following parameters for the interrogation areas: final interrogation area size of 32×16 pixels in the horizontal and vertical directions, respectively, no overlap between neighbour interrogation areas, one refinement step, and an initial interrogation area size is of 64×32 pixels. The validation parameters used are: moving average validation with an acceptance factor of 0.15 with three iterations using a neighbourhood size of 3×3 . The adaptive correlation on the right of Figure 6 used the following parameters for the interrogation areas: final interrogation area size of 32×32 pixels, 25% and 50% of horizontal and vertical overlap, respectively, and five refinement steps using an initial interrogation area size of 1024×1024 pixels. The validation parameters used are: minimum peak height relative to peak 2 of 1.2, moving average validation using 3 iterations using a neighbourhood size of 3×3 and an acceptance factor of 0.15.